V European Conference on Computational Fluid Dynamics
ECCOMAS CFD 2010
J. C. F. Pereira and A. Sequeira (Eds)
Lisbon, Portugal,14-17 June 2010

NUMERICAL TREATMENT OF CONTACT LINE MOTION NEAR A SHARP CORNER

Poorya A. Ferdowsi* **and Markus Bussmann†**

University of Toronto,
Department of Mechanical and Industrial Engineering
*e-mail: p.ferdowsi@utoronto.ca
†e-mail: bussmann@mie.utoronto.ca

Key words: Multiphase flow, Volume-of-fluid, Contact angle, Corner

Abstract. *Approaches to modeling contact line motion within the volume-of-fluid method are always presented for a flat surface. But what if a surface is geometrically more complex, and, for example, contains a sharp corner? Here we present an algorithm for modeling contact line motion around a sharp corner, by pinning an advancing contact line at the corner, allowing the contact angle to increase and the contact line to rotate around the corner, and then releasing the contact line when the contact angle has reached the value associated with the other side of the corner. We present the algorithm details in the context of the EI-LE advection method, and then present preliminary results that illustrate the methodology.*

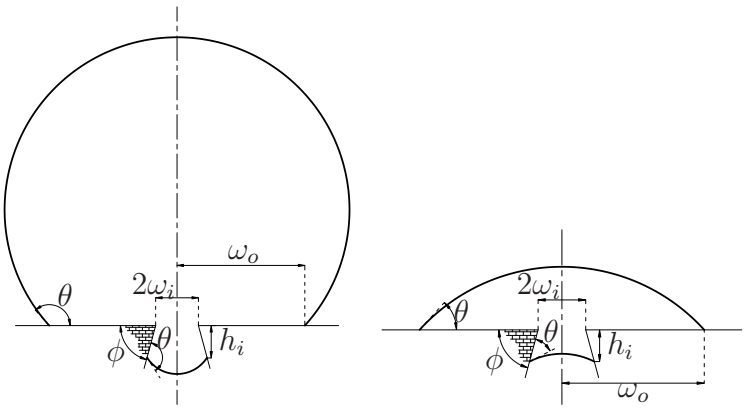

Figure 1: Two configurations of a droplet seated coaxially above an open pore, corresponding to two different θ. The hatched area is a smooth solid.

1 INTRODUCTION

Contact line motion is an integral part of interfacial flows when a solid surface is in contact with a liquid-gas interface (e.g. spray coating, ink-jet printing). Typically the contact line moves over a continuous solid surface, but when the surface is geometrically more complicated, for example, than a flat surface, then equilibrium interfacial configurations may be metastable, because the configuration will depend on the way that equilibrium is reached. Consider, for example, a droplet seated on a single pore in a surface, as depicted in figure 1. To simulate the droplet flow into the pore, and to predict the final equilibrium configuration, it is necessary to consider the effect of the sharp corner on the motion of the contact line. In this article we examine exactly this scenario: the numerical simulation of contact line motion at a sharp corner. The key to such a simulation is a treatment of the sharp corner that is solely dependent on the geometry of the corner and on the contact angle, based on the concept of contact line pinning [6].

For numerical simulation of immiscible incompressible two-phase Newtonian flow, an interface tracking algorithm is usually combined with a flow solver. Among numerous

methods devised for simulating two-phase flows, the volume-of-fluid (VoF) scheme is one that preserves the volume of each component exactly [8, 9]. In the work presented here, the mathematical model is based on a one-field approach: the Navier-Stokes (N-S) equation is solved over the entire domain, alongside an advection equation for the VoF field. The N-S equation is:

$$\partial_t(\rho\vec{V}) + \partial_{\vec{x}} \cdot (\rho\vec{V}\vec{V}) = -\partial_{\vec{x}} p + \vec{F}_S + \vec{F}_B \tag{1a}$$

$$\partial_{\vec{x}} \cdot \vec{V} = 0 \tag{1b}$$

where $\vec{V}$ is the velocity field, p is the pressure field, $\vec{F}_S$ represents the surface forces including viscous effects, $\vec{F}_B$ represents any body forces such as gravity, ∂_t represents the derivative with respect to time and $\partial_{\vec{x}}$ represents the gradient operator. In equation (1a) $\rho = \sum f_k \rho_k$ and $\mu = \sum f_k \mu_k$ where f_k is the volume fraction of phase k. The balanced force CSF method is used for modeling the surface tension force [5]. The numerical solution of the N-S equation is obtained by a projection method [3, 5, 2].

In a two-phase flow, if the volume fraction of the first phase is designated by f, that of the second phase is $1-f$, and so only one governing equation for the interface is required. For a given velocity field, the volume fractions are advected by:

$$\partial_t f + \vec{V} \cdot \partial_{\vec{x}} f = 0 \tag{2}$$

Since these f values are discontinuous, the numerical solution of equation (2) must be treated carefully. Many Eulerian and Lagrangian advection schemes have been suggested to solve this equation [8, 9, 11]. In this article, the solution to this equation is of interest when the contact line is near a sharp corner. We address such a treatment here, and

investigate the accuracy of the presented technique.

2 THEORY

Since treatment of the sharp corner is performed within a VoF framework, we briefly present the interface reconstruction and advection schemes that we implemented. The interface reconstruction method is PLIC, in which the interface is represented by piecewise linear segments [8]; these segments are then advected by the operator split EI-LE method of Scardovelli et al. [11].

2.1 INTERFACE RECONSTRUCTION AND ADVECTION

In order to reconstruct an interface via PLIC, an interface normal and a line constant are required. Given the normal, the unique line constant can be computed explicitly [10]; normals can be computed in many ways [9]. For simplicity, we use the height function (HF) method to compute both normals and curvatures [4]. The HF technique computes the interface normal by calculating fluid "heights" in a 7×3 stencil, and then calculating the central difference of these heights (see figure 2). The orientation of the stencil should be most normal to the interface, and so a simple estimate of the normal (e.g. Parker and Youngs [7]) is used to estimate stencil orientation. Assuming that the interface is more horizontal than vertical, three fluid heights are defined as:

$$H_{i+\alpha} = \sum_{\beta=-3}^{3} f_{i+\alpha,j+\beta} \Delta y_{j+\beta} \quad \text{for } \alpha = -1, 0, 1 \tag{3}$$

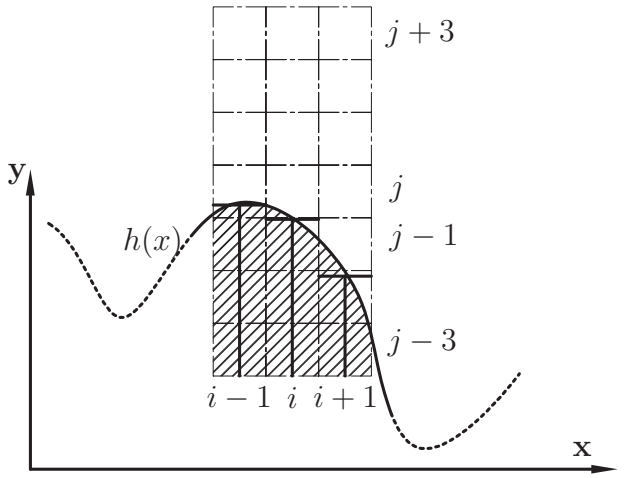

Figure 2: Heights H_{i-1}, H_i and H_{i+1} for the interface cell (i, j).

where Δy is the vertical dimension of a cell. The interface normal is then obtained by the central difference technique:

$$\begin{aligned} n_x &= H_{i+1} - H_{i-1} \\ n_y &= x_{i+1} - x_{i-1} \end{aligned} \tag{4}$$

and curvature evaluated as:

$$\kappa = \frac{\ddot{y}}{(1 + \dot{y}^2)^{\frac{3}{2}}} \tag{5}$$

where $\dot{y} = n_x/n_y$, and $\ddot{y}$ is the numerical discretization of the second order derivative.

When the interface normal and curvature are required near a solid phase, close to a contact line, we use the extended HF method of Afkhami et al. [1], where the interface is first reconstructed in the contact line cell[1] and then extended into the solid. The volume fractions is the ghost cells are obtained by extrapolating a linear approximation of the interface after which the HF method can be applied as usual.

After reconstructing the interface at each timestep, it must be advected by the velocity

[1] a cell containing a three-phase line (in 2D this appears as a point).

field. We used the split EI-LE method [11], since it preserves mass exactly and is consistent (i.e. no "wisps" appears in the solution). The volume fraction advection equation (2) is discretized into an implicit Eulerian step in one direction:

$$f_{i,j}^{(n+\frac{1}{2})} = \frac{f_{i,j}^{(n)} + F_l^{(n)} - F_r^{(n)}}{1 + u_l - u_r} \tag{6}$$

followed by a Lagrangian explicit step in the other:

$$f_{i,j}^{(n+1)} = f_{i,j}^{(n+\frac{1}{2})}(1 + u_l - u_r) + G_t^{(n+\frac{1}{2})} - G_b^{(n+\frac{1}{2})} \tag{7}$$

F_l, F_r, G_b and G_t are the fluxed fractions from the left, right, bottom and top faces of the cell (i, j), respectively, that are computed based on the reconstruction at each level; u_l and u_r are the Courant numbers at the left and right faces of the cell (i, j). In the Lagrangian step, the faces of the cell are advected first, and then the fluxed fractions are calculated (i.e. G_t and G_b); during the Eulerian step, the fluxed fractions F_l and F_r are computed first and then the interface is advected (see figure 3). After each sweep, the interface is reconstructed. Finally the order of the sweep direction alternates with each timestep.

2.2 SHARP CORNER TREATMENT

In this section we explain how the advection scheme must be amended when the contact line is near a sharp corner, as shown in figure 4. The method is based on the concept of contact line pinning [6]: when the contact line reaches an ideally sharp corner, it pins itself there and then rotates about the corner until it reaches the contact angle on the other side, as illustrated in figure 4.

To model this phenomenon, we compute the apparent contact angle based on the

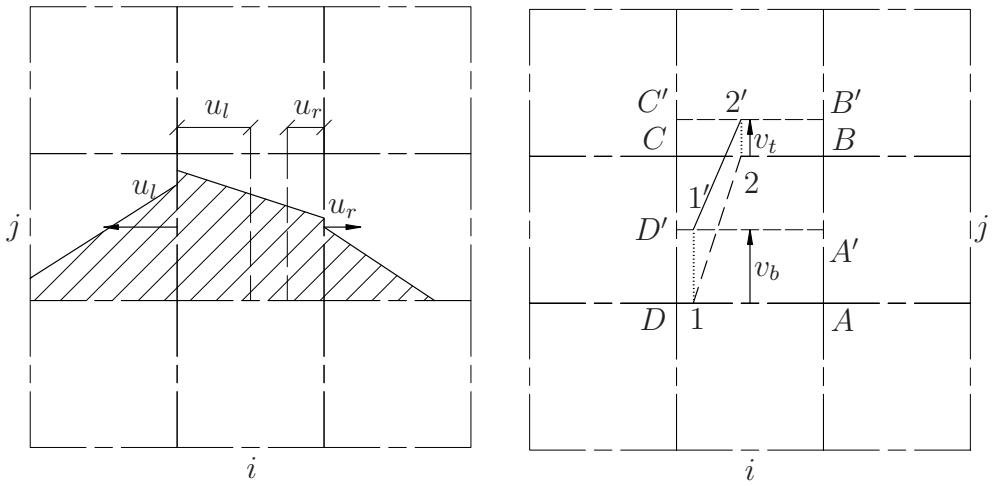

(a) EI (b) LE

Figure 3: (a) The net outward flux areas used in the EI step are calculated by intersecting the total outflux rectangles within the shaded fluid region. (b) In the LE step, the faces of the cell are advected first along the advection direction; then the net outflux is calculated. $BB'C'C \bigcap B'2'1'A'$ is the net outflux through the top face.

volume fraction of the contact line cell. Here, for the sake of simplicity, we consider a wall angle $\phi = \frac{\pi}{2}$. We also assume that the contact angle on a smooth surface, $\theta < \frac{\pi}{2}$. Now, we modify the advection scheme and compute the apparent contact angle θ_a when the contact line is pinned to the sharp corner, as shown in figure 5.

Suppose that the contact line has reached the sharp corner. Cells (i, j) and $(i - 1, j)$ must be treated differently; other configurations can be treated similarly. For now,

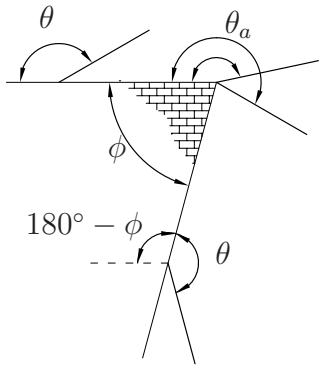

Figure 4: A contact line at a corner, and the limits of the apparent contact angle.

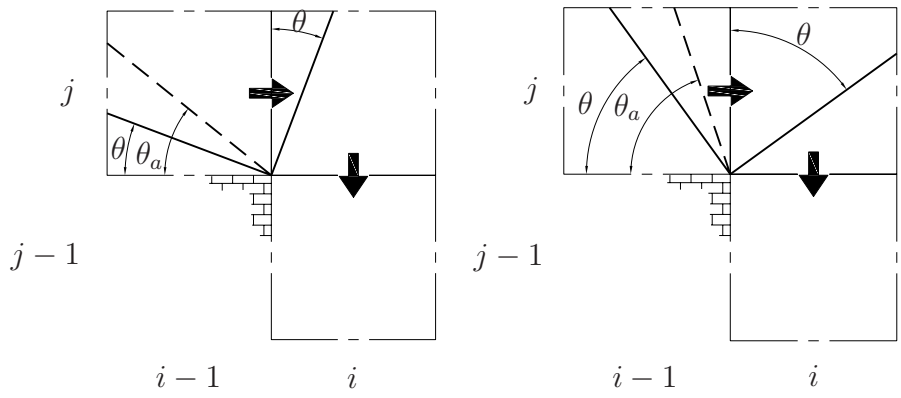

(a) $\theta < \frac{\pi}{4}$ (b) $\frac{\pi}{4} < \theta < \frac{\pi}{2}$

Figure 5: The pinned contact line for two different θ. The dashed line is the reconstructed interface after one time step. θ_a is the new contact angle in the contact line cell where the contact line is pinned.

suppose that the contact line is in cell $(i-1, j)$, pinned to the sharp corner, and that the contact angle is $\theta_a \geq \theta$. In this case, for a square mesh, the corresponding pinned volume fraction f_p is:

$$\begin{cases} \theta_a < \dfrac{\pi}{4} & \Rightarrow \quad f_p = \dfrac{1}{2}\tan\theta_a \\ \theta_a \geq \dfrac{\pi}{4} & \Rightarrow \quad f_p = 1 - \dfrac{1}{2}\cot\theta_a \end{cases} \tag{8}$$

Notice that, when the contact angle is assumed to be pinned to the corner, the only fluid that ought to cross the right face is the gas phase. So, for advection in the x direction one can compute a temporary fraction f^* based on the EI-LE method assuming that no fluid leaves the right face; that is $F_r^{(n)} = 0$ in equation (6). (A similar approach would be required for Lagrangian advection in the x direction). For advection in the y direction, both phases can flux through the top face. If the temporary fraction $f^* \in [f_p, 1]$, then $f^{(n+1)} = f^*$, and one can calculate the apparent contact angle as follows:

$$\begin{cases} f^* < \dfrac{1}{2} & \Rightarrow \quad \theta_a^{(n+1)} = \tan^{-1}\big(2f^{(n+1)}\big) \\ f^* \geq \dfrac{1}{2} & \Rightarrow \quad \theta_a^{(n+1)} = \cot^{-1}\big(2(1-f^{(n+1)})\big) \end{cases} \tag{9}$$

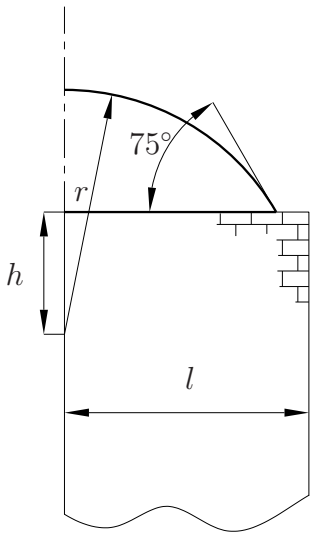

Figure 6: Geometric parameters.

If $f^* \notin [f_p, 1]$, then one computes $f^{(n+1)}$ as usual by releasing the pinned contact line, thereby allowing any fluid to flux out of the right face of the cell $(i-1, j)$.

When the interface is in the cell (i, j), and when the contact line is pinned, similar to the previous discussion, only the phase corresponding to $f = 0$ can leave the bottom face. So, $G_b^{(n+\frac{1}{2})} = 0$ in equation (7) (similarly for Eulerian advection in the x direction). In this case, equation (8) is still valid, but if $f^* < f_p$ the contact line can remain pinned to the edge, and $\theta_a^{(n+1)}$ is calculated by equation (9); otherwise, the contact line must be released, and the new volume fraction can be computed as usual.

Finally, knowing θ_a one can reconstruct the interface in the contact line cell and then calculate the interface curvature as usual.

3 RESULTS

In this section we investigate the ability of the method we have presented, for treating contact line motion near a sharp corner. Consider a sessile drop on a pedestal, with an initial contact angle $\theta = 75°$, as illustrated in figure 6. Due to symmetry, only half of the

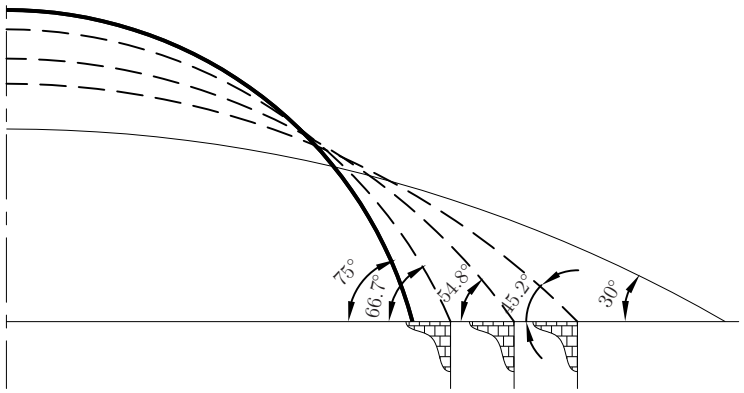

Figure 7: Equilibrium configuration for different corner positions.

domain is considered. Then the contact angle is suddenly changed to $\theta = 30°$. We run the simulation for three different pedestal sizes.

The fluids used in this simulation are water and air. Surface tension coefficient $\sigma = 728$ N/m. Geometric parameters are $h = 4.732 \times 10^{-1}$ m and $r = 1.035 \times 10^{-1}$ m. The domain is a 0.5×1 m^2 rectangle and the grid size is fixed at $\Delta = \frac{1}{32}$. The pedestal width l is set to 7Δ, 8Δ and 9Δ. The Poisson solver uses a two-level preconditioned GMRES technique. Machine accuracy is assumed to be 10^{-13} which is also set as the convergence tolerance for the GMRES solver.

From a thermodynamic viewpoint, in the absence of a sharp corner, the drop will spread over the surface and oscillate until it reaches to an equilibrium configuration. But, in presence of the sharp corner, the droplet instead pins to the edge [6] . These equilibrium configurations are depicted in figure 7. Simulation results are shown in figure 8 at three different times. We see that the equilibrium configuration predicted numerically is in good agreement with the thermodynamic one. Due to spurious currents which are induced by inaccuracies in the curvature computation, the interface is still vibrating about the corresponding exact interface, even after 5 seconds. We see that by changing the pedestal size, it is possible to control the equilibrium contact angle at the pinned corner as well

as the maximum spread. For wider pedestals, equilibrium contact angles are smaller. In none of these cases, does the drop wet the vertical side of the pedestal.

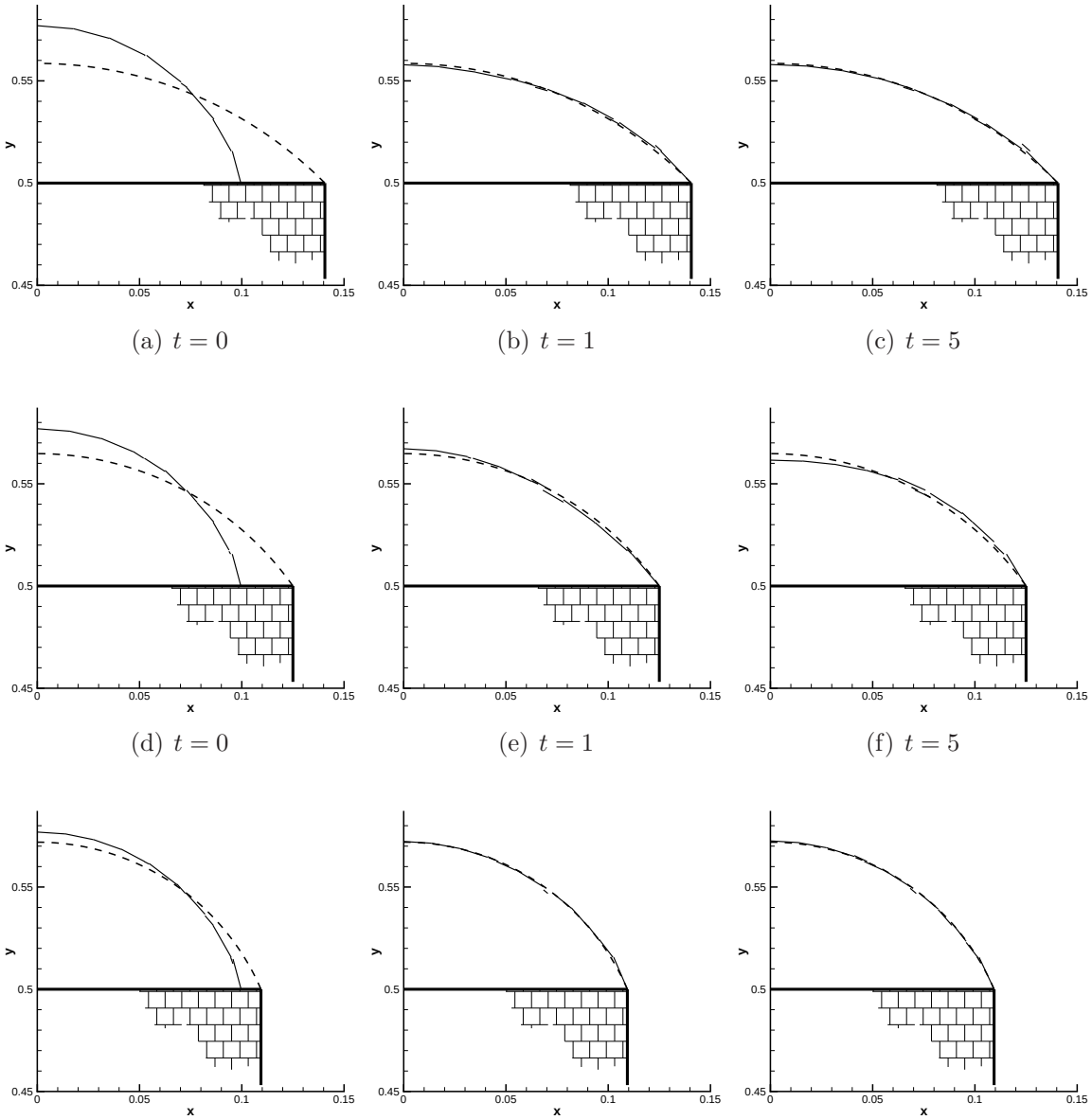

(a) $t = 0$ (b) $t = 1$ (c) $t = 5$

(d) $t = 0$ (e) $t = 1$ (f) $t = 5$

(g) $t = 0$ (h) $t = 1$ (i) $t = 5$

Figure 8: (a)-(c) Results at three steps when $l = 9\Delta$; (d)-(f) when $l = 8\Delta$; (g)-(i) when $l = 7\Delta$. The exact equilibrium configuration is shown by the dashed line; the numerical results are shown by the solid line. $\Delta = 1/32$ is the grid size.

REFERENCES

[1] S. Afkhami and M. Bussmann. Height functions for applying contact angles to 2D VOF simulations. *International Journal for Numerical Methods in Fluids*, 57(4):453–472, 2008.

[2] M. Bussmann, D.B. Kothe, and J.M. Sicilian. Modeling high density ratio incompressible interfacial flows. *"Proceedings of FEDSM02 ASME Fluids Engineering Division Summer Meeting"*, 2002.

[3] A. J. Chorin. Numerical solution of the Navier-Stokes equations. *Mathematics of Computation*, 22(104):745–762, 1968.

[4] S. J. Cummins, M. M. Francois, and D. B. Kothe. Estimating curvature from volume fractions. *Computers and Structures*, 83(6-7):425–434, 2005.

[5] M. M. Francois, S. J. Cummins, E. D. Dendy, D. B. Kothe, J. M. Sicilian, and M. W. Williams. A balanced-force algorithm for continuous and sharp interfacial surface tension models within a volume tracking framework. *Journal of Computational Physics*, 213(1):141–173, 2006.

[6] J. F. Oliver, C. Huh, and S. G. Mason. Resistance to spreading of liquids by sharp edges. *Journal of Colloid and Interface Science*, 59(3):568–581, 1977.

[7] B.J. Parker and D.L. Youngs. Two and three dimensional Eulerian simulation of fluid flow with material interfaces. *UK Atomic Weapons Establishment*, 01/92, 1992.

[8] W. J. Rider and D. B. Kothe. Reconstructing volume tracking. *Journal of Computational Physics*, 141(2):112–152, 1998.

[9] R. Scardovelli and S. Zaleski. Direct numerical simulation of free-surface and interfacial flow. *Annual Review of Fluid Mechanics*, 31:567–603, 1999.

[10] R. Scardovelli and S. Zaleski. Analytical relations connecting linear interfaces and volume fractions in rectangular grids. *Journal of Computational Physics*, 164(1):228–237, 2000.

[11] R. Scardovelli and S. Zaleski. Interface reconstruction with least-square fit and split Eulerian-Lagrangian advection. *International Journal for Numerical Methods in Fluids*, 41(3):251–274, 2003.